Egypt. J. Phys. **Vol. 51,** pp. 21-33 (2023)

Egyptian Journal of Physics

https://ejphysics.journals.ekb.eg/

Measuring The Fraction of Electromagnetic Energy as Probe Collective Effects in p-p Collisions at 13 TeV

Hadeel E. Salem[1], A.M. Basha[1], M.A. Mahmoud[1], Ralf Ulrich[2], Y. Mohammed[1]

[1]*Center for High Energy Physics (CHEP-FU), Physics Department, Faculty of Science, Fayoum University, 63514 El-Fayoum, Egypt*

[2]*Karlsruhe Institute of Technology (KIT), Germany*

Abstract

The very forward region (-6.6 ≤ η ≤ -5.2) is cover by CASTOR detector, that region cannot be covered by CMS experiment. As a function of pseudorapidity, a measurement of the fraction of electromagnetic energy used to explore collective effects in proton-proton collisions at energy √s = 13 TeV is reported. Data was compared using various Monte Carlo generators. In contrast to the data, each model under consideration suggests a distinct form for the pseudorapidity dependence. Additionally, systematic studies have also been performed. Further sources of uncertainties related to detector and analysis were found and quantified. It was shown that the calorimeters of CMS taken all together and covering a very wide eta range from |0.0| to |6.6| may well be suited to provide further insights into hadronization and collective effects even in Zero Bias p-p collisions. Several comparisons with MC simulations show that the facts are well-described. Also, MC was utilized to calculate the correction factors from detector-level to particle-level.

1. Introduction

The basic task of Quantum Chromo-Dynamics (QCD) is to describe inelastic proton-proton collisions by combining hard and soft exchanges between the components of protons. Soft parton scattering from Multiple Parton Interactions (MPI) [1–4] complements hard collisions involving one or more pairs of partons. Initial-state and final-state radiation, as well as projectile fragmentation, make up the underlying event (UE) in parton showers [5]. The LHC experiments investigated these effects at the greatest center-of-mass energies achieved in lab, which span a wide angular phase space. The average energy per p-p collision measured at various pseudorapidity (η) areas elucidates our overall knowledge of multiparticle generation. Furthermore, smaller scattering angles may be obtained compared to other observations due to the CMS experiment's expanded calorimeters beyond |η|>3, encompassing the complete range from 6.6 to +5.2 in pseudorapidity.

The fraction of electromagnetic energy as collective probe effects in proton-proton collisions at 13 TeV is measured in the present work. The present paper can be considered an extension of previous results from the CMS [6], ATLAS [7], and LHCb [8] Collaborations in the energy and η range covered. The definition of average energy density per collision is:

$$\frac{dE}{d\eta} = \frac{1}{N_{coll}} \sum_i E_i \frac{c(\eta)}{\Delta\eta} \qquad (1)$$

where $\sum_i E_i$ is the total (summed) energy measured for all calorimeter towers i within a bin of pseudorapidity having a width Δη, c(η) is the η-dependent conversion factor from the calorimeter measurements to a stable- level particle energy, and N_{coll} refers to the number of selected p-p collisions were corrected for the contributions from

*Corresponding author: *e-mail: hadeel.ezzeldeen@cern.ch

DOI : 10.21608/EJPHYSICS.2022.150351.1082

Received: 15/7/2022; accepted: 9/8/2022

noise and simultaneous p-p collisions occurring in the same event. The measurement is done for various different categories of collisions with varied event selections to examine various features of multi parton interaction (MPIs) at high-energy p-p collisions.

The present analyzed data is important because projectile fragmentation may then be studied in regions near the beam rapidity, y_{beam}=a cosh ($\sqrt{s}/2m_p$), where m_p is the mass of the projectile particle, which in this instance is a proton; hence at $\sqrt{s}$=13 TeV, $y_{beam}\approx 9.5$. When data acquired at multiple center-of-mass s energies are merged, the detectors of CMS, despite being stationary, cover a very large range in y_{beam}. According to the limiting fragmentation theory [9], particle production displays longitudinal scaling, i.e, the dependency of extremely forward particle production on the energy diminishes in the area $\eta\approx 0$ [10].

2. The CMS detector

Superconducting solenoid with a 3-m internal radius, it could generate a magnetic field with strength of 3.8 T located at the heart of the CMS detector. An inner silicon pixel and strip tracker measuring charged particles in the range $|\eta|\leq 2.5$, electromagnetic calorimeter, and hadron calorimeter are all contained within the CMS magnet. With tracking and calorimetry, the associated endcap detectors span the pseudorapidity range up to $|\eta| \leq 3$. Cherenkov calorimeters in the forward direction expand the coverage past $|\eta| \geq 3$. Gas-ionization detectors placed in the steel return yoke are used to measure muons.

The hadron forward calorimeter (HF) has 2×432 readout towers and it covers the region $2.9\leq|\eta|\leq 5.2$. Each tower has a steel absorber that runs parallel to the beam and contains long and short quartz fibres.

In pseudorapidity ($-6.6 \leq \eta \leq -5.2$), the CASTOR calorimeter covers a single side of CMS at extremely forward angles. It consists of 16 azimuthal towers, each tower comprised of 14 longitudinal modules. The electromagnetic part comprises two front modules, whereas the hadronic section is made of 12 rear modules. Two half-cylindrical mechanical structures make up the calorimeter. It consists of stacked tungsten and quartz platesread by photomultiplier tubes PMTs. The calorimeter is placed around the beam pipe at a distance of - 14.4 meters from the point of interaction. CASTOR and HF both have a total longitudinal depth of 10 hadronic interaction lengths.

The CASTOR calorimeter is used when the LHC luminosity is low ($\mathcal{L}_{inst} < 10^{30}$cm^{-2}/s); therefore, it can't tell the difference between secondaries and pileup collisions. The scope of this study is limited to the range covered by HF calorimeter and CASTOR calorimeters, with the exception of the two lowest $|\eta|$ segments of the HF calorimeters, which are partially shielded by the endcap calorimeters, this η-range combined the two ranges of $3.15\leq|\eta|\leq 5.2$ and $-6.6\leq|\eta|\leq -5$. The study was done using an integrated luminosity ⌊ of 0.06 nb^{-1} and an average number of p-p interactions per bunch crossing of around 0.05. [11]

3. Monte Carlo and data

Different Monte Carlo event generators were utilized in this research to adjust the data from the detector to the stable-particle level and compare it to the experimental results. PYTHIA 8 [12] event generator is a general-purpose Monte Carlo software that bases the majority of its predictive capacity on hard-scattering matrix elements derived in perturbative QCD and Parton showers using the Dokshitzer–Gribov–Lipatov–Altarelli–Parisi (DGLAP) equations [13–17]. For hadronization, the string fragmentation model is utilized [18]. In addition, the simulations' free parameters were modified to describe data at different collision energies, resulting in different model tunes [19].

In this study, PYTHIA 8 is combined with the CUETP8M1 [19]. Furthermore, the parameters are tweaked to describe the underlying event at LHC data .

The massive air showers in the atmosphere brought on by cosmic ray particles are described by the EPOS-LHC event generator [20], where soft physics is of utmost importance. This model is based on perturbative QCD, string fragmentation, and Gribov-Regge multiple scattering (21). Greater adjusting opportunities are offered by the phenomenology used in EPOS-LHC. In EPOS-LHC [20], a hydrodynamic, or collective, component is integrated in a parameterized manner.

The ZeroBias1 Run2015A data is a beam bunch crossing-time trigger that produces a "zero bias" dataset with 100% efficiency. In addition to the possibility of collecting events with real collisions, only active beam bunch crossings are read out.

4. Particle level definition

..

The event selected at generator level (particle level) by the following criteria:

Soft inclusive events are selected by $\xi=\max(\xi X, \xi Y) > 10^{-6}$, where ξ is defined in equation (2). There are two classification methods for all particles. The largest rapidity gap in the event is attributed to system X on the negative side, and system Y is responsible for the positive side's particles. The invariant masses of the two systems are MX and MY; their ratios to the squared center-of-mass $\sqrt{s}$ energy ,ξX and ξy , are defined as:

$$\zeta_X = \frac{M_X^2}{s}, \zeta_Y = \frac{M_Y^2}{s} \qquad (2)$$

Non-single-diffractive(NSD) events in the simulation are selected with a requirement of at least one stable particle (even charged or neutral) with E > 5 GeV within the pseudorapidity acceptance of the HF calorimeters, $3.15 \leq |\eta| \leq 5.20$ on both side of the interaction point IP .for comparison to previously published result [22], Non-Single Diffractive enhanced (NSD-enhanced) events are also selected with the requirement of at least one charged particle on both sides of the interaction point IP in η-range $3.9 \leq |\eta| \leq 4.4$.

The Single Diffractive enhanced (SD-enhanced) events at the particle level are defined by the presence of at least one stable particle with energy E > 5 GeV with η-range $3.15 \leq |\eta| \leq 5.2$ on one side, while the other side has to be devoid of particles with energy E > 5GeV. The transverse energy at the detector level is calculated using the energy and simple geometrical factor, $\sin(\theta)$, for each η- bin. At the particle level, the component of the four momenta of every particle is used to build sums of transverse energies. The phase space defined for soft inclusive inelastic, non-single diffractive enhanced (NSD-enhanced), and single diffractive enhanced (SD-enhanced) events on particle level are summarized in Table 1.

Table 1. Summary of particle level definitions for each event selection: inelastic, NSD-enhanced and SD-enhanced event selection

Inelastic	$\xi > 10^{-6}$
NSD-enhansed	At least one stable particle with E>5GeV in $3.15 < \|\eta\| < 5.20$, on both sides of the interaction point (IP).
SD-enhanced	At least one stable particle with $E > 5$ GeV in $3.15 < \|\eta\| < 5.2$ on one side, while the other side particle with $E < 5$ GeV.

5. Calorimeter noise level from data

In this section, we summarize calorimeter level results obtained from Mont-Carlo collision data and empty bunch crossing data (EmptyBX). In Fig. 1, comparisons spectra of energy distributions of hadron particles at different eta bins. (data_ZeroBias1) and empty data (data_L1TechBPTXQuiet) is presented. In all of the eta bins, the distributions are normalized to the total number of events in the sample. Data and MC simulation are constituent each other in particular at high values of energy. The empty data (data_L1TechBPTXQuiet) and (data_ZeroBias1). We observe that the energy distribution increase with increasing of eta-bin number. In figures 2, 3, we present comparisons of energy spectra distribution of electromagnetic particles at different eta of bins from eta-bin=0 to eta-bin=10, the (data_ZeroBias1) with simulation from MC event generator (PYTHIA8 and EPOS-LHC). There is a few different observations between the Hadronic and electromagnetic particles energy distribution.

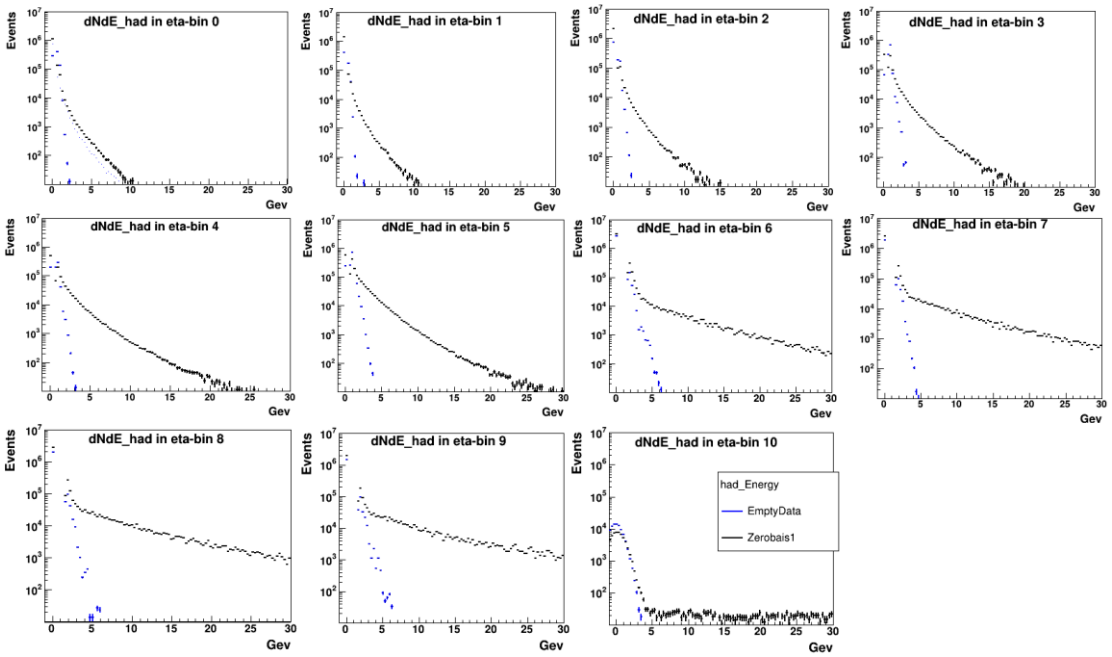

Fig. 1. Comparison of hadron particle energy distributions (data-zerobias) and empty-data (L1TechBPTXQuiet). Overemphasizes the nois region, which for example for dNdEeta_bin 10 leads to large purely visual discrepancy.

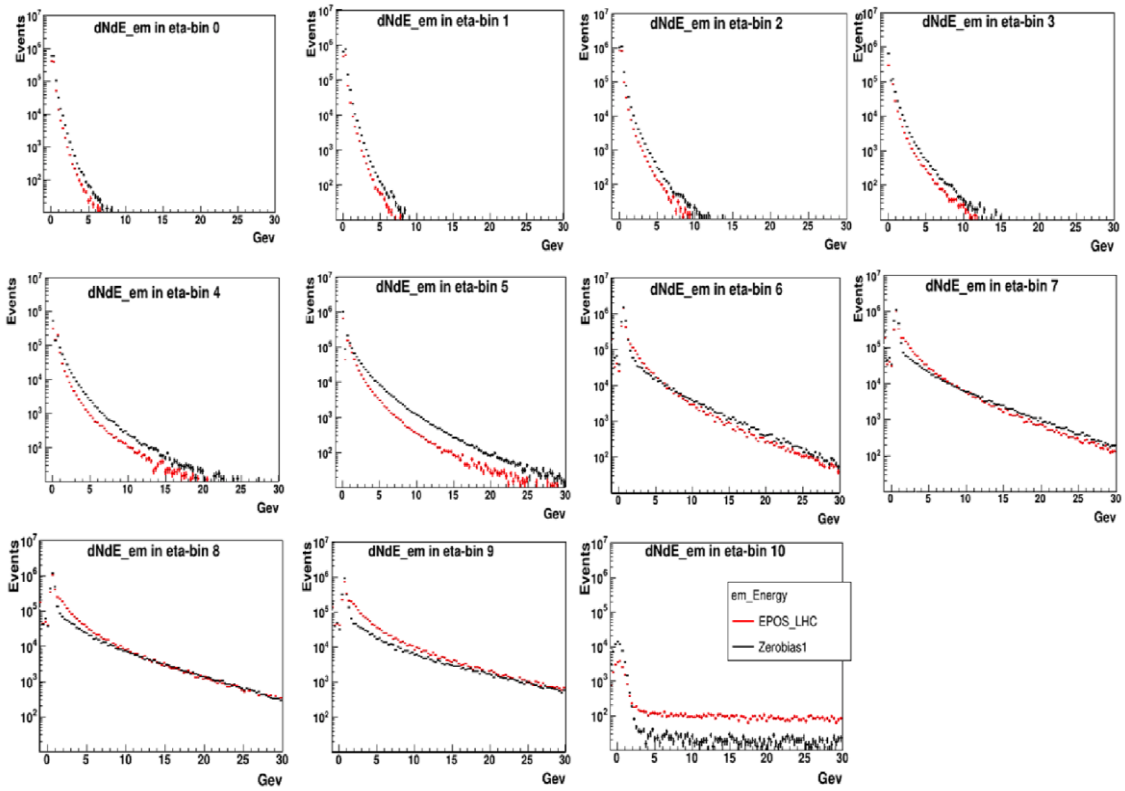

Fig. 2. Comparison of electromagnetic particle energy distributions (data-zerobias) and MC-data (EPOS-LHC). Overemphasizes the nois region, which for example for dNdEeta_bin 10 leads to large purely visual discrepancy.

..

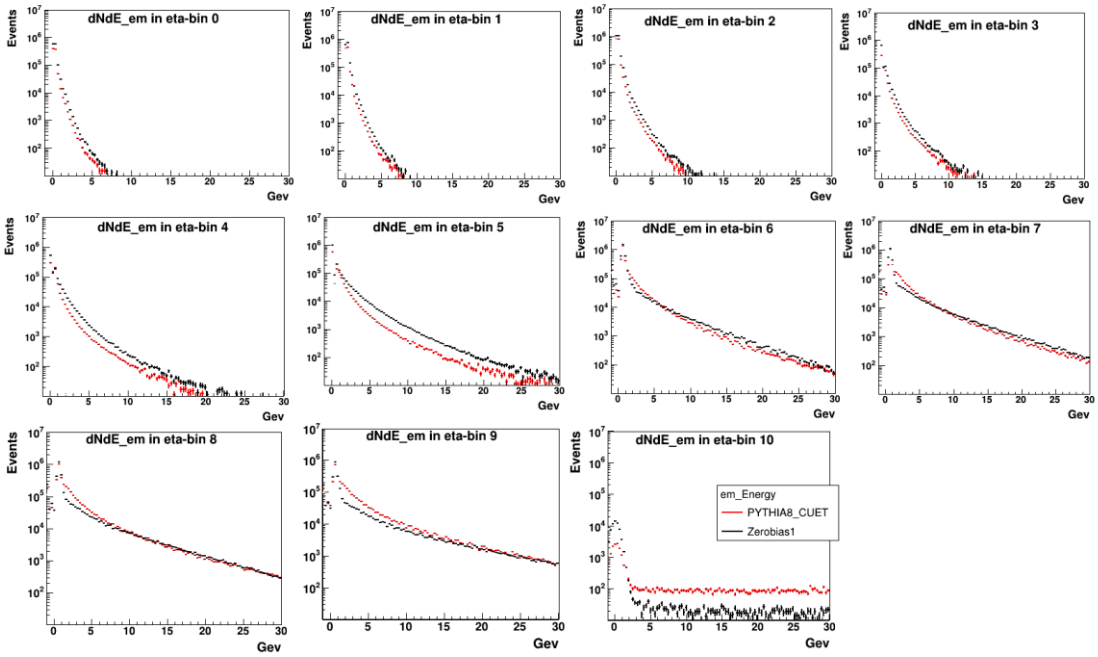

Fig. 3. Comparison of electromagnetic particles energy distributions (data-zero-bias) AND MC-data (PYTHIA8_CUET). Overemphasizes the nois region, which for example for dNdEeta_bin 10 leads to large purely visual discrepancy

6. Corrections from detector level to generator level

The calorimeter of CMS measures the properties of distribution of particle generated at the interaction point only indirectly. The distributions are affected by dead material, detector segmentation calorimeter compensation inefficiencies, resolution and to an important degree by detector noise. The data is corrected from detector level to generator level by using (PYTHIA8_CUET, PYTHIA8_MBR, and EPOS-LHC) MC event generators with the simulation of the CMS detector data based on GEANT4. The correction bin-by-bin factor is calculated as ratios of the average of MC prediction at the generator and detector level.

In this analysis we study the efficiency or bin-by-bin correction factor; firstly we have to calculated the corrected energy measurements in order to produce and compute high accurate energy, then the correction energy are the ratios of the average of MC predictions at generator level and detector level multiplied to the energy of detector level of CMS data, in the same way as they were used in the previous similar CMS analysis [22]. In what follows we argue in favor of such a procedure compared to iterative unfolding techniques using response matrices. No quickly changing distribution is involved in our studies. The uncertainties are fully dominated by relatively large systematic on global calorimeter energy scale, there is only minimal cross-talk between different eta bins due to finite shower size when a shower from one cell leaks to the neighboring cell but a leak in one direction is compensated by another leak in the opposite direction factor from the detector level to the generator level. The comparison of the detector level and generator level of hadronic particle energy flow in figure 4 and electromagnetic particle energy flow in figure 5 for various MC predictions. Figure 4, according to the average correction factor, as shown the correction factor in CASTOR range is (≈<1) this refer to underlying events inside the detector.

In hadronic particle case, the amount of dead material and beam bump crossing effect in the range $0.0 \leq |\eta| \leq 1.0$ and the leakage of the shower in rang $2.5 \leq |\eta| \leq 3$, figure 5, according to average correction factor, as shown the correction factor in CASTOR range is (≈2).

While at the detector level there is a large variation of prediction between different MC models, the variation of the correction factor is smaller indicating than the magnitude of detector effects (non–compensation of calorimeter) plays the major role. To assess the model dependency as a systematic effect, the envelope maximum variation of correction factor value is obtained using 3 different MC samples.

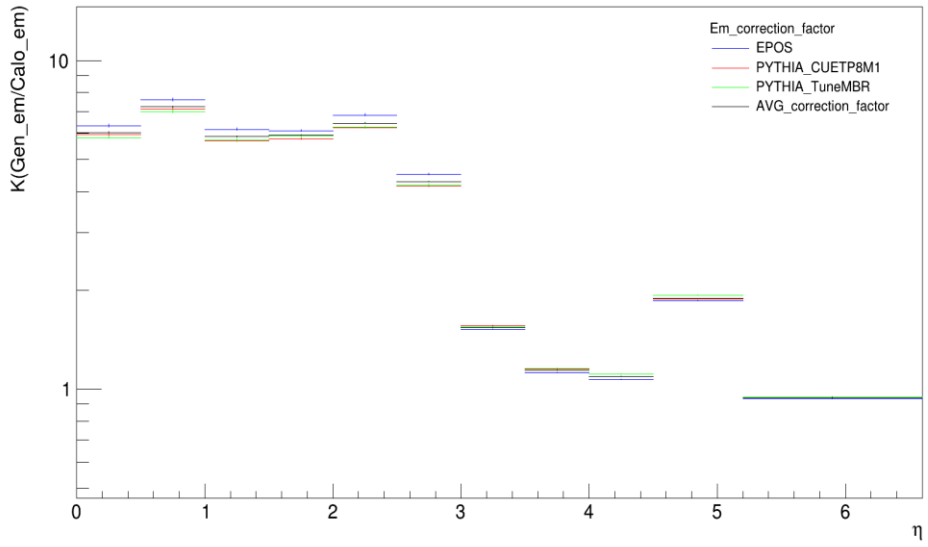

Fig. 4. Comparison between the ratio of detector level (for electromagnetic particles and generator level for various MC predictions (correction factor).

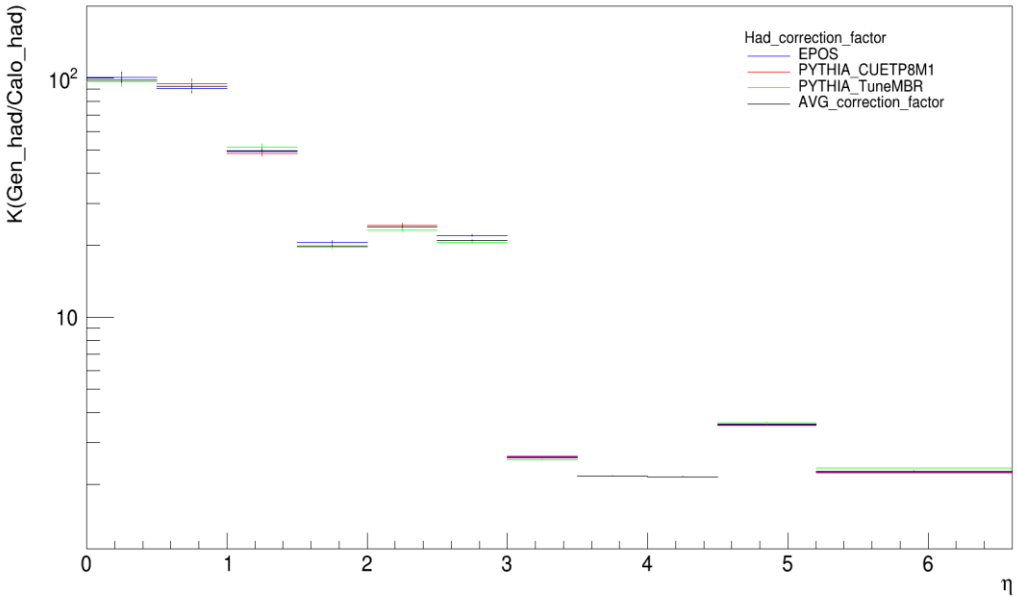

T

Fig. 5. Comparison between the ratio of detector level (for hadronic particles) and generator level for various MC predictions (correction factor).

7. Systematic uncertainty errors

The statistical errors may be small and will never show, the systematic uncertainly errors is just statistic of the data and MC models it may be 1% or smaller, we choose a specific cross section 3.6<|□ |<5.2 anddefine the error percentage in Table 2:

..

Table 2. Systematic uncertainty errors percentage

Systematic uncertainty source	Statistical error of data and MC			
	EPOS_LHC	PYTHIA_LHC	PYTHIA_MBR	Corr_Avg
Noise threshold	2.7%	<1%	<1%	9.4%

As shown the errors in case of PYTHIA8_MBR &PYTHIA8_CUET are almost the same.

8. Compatibility

In the present section, the comparison between MC models (EPOS_LHC, PYTHIA8_CUET, PYTHIA8_MBR) to see which one is good enough TO describe the real data or which of them is more compatible with the real data (Zero_Bias2). In figure 6 appears the ratios between all chosen MC models (EPOS_LHC, PYTHIA8_CUET, PYTHIA8_MBR) to the real data (Zero_Bias2) in case of energy distribution of reconstructed electromagnetic particles. As shown in figure 6 all ratios are up to 1 -this is acceptable- but the most approach MC model to 1 is the most suitable model compatible with the real data; as shown in pseudorapidity $0.0<|\eta|<2.8$ the EPOS_LHC model is the most compatibility with the real data, the pseudorapidity $3.0<|\eta|<4.4$. MC model PYTHIA8_CUET is the most compatibility with the real data, but in the pseudorapidity $4.4<|\eta|<5.2$ MC model PYTHIA8_MBR is most compatibility with real data.

In Fig. 7 appears the ratios between all chosen MC models (EPOS_LHC, PYTHIA8_CUET, PYTHIA8_MBR) to the real data (Zero_Bias2) in case of energy distribution of reconstructed hadronic particlesratios is approaching to 1 than electromagnetic particles, that is refer to the MC models are more compatible with real data in case if hadronics particle than the electromagnetic particles to describe the real data, as shown in Fig. 7 the MC model PYTHIA8_CUET is the most compatible model with the real data than the other models.

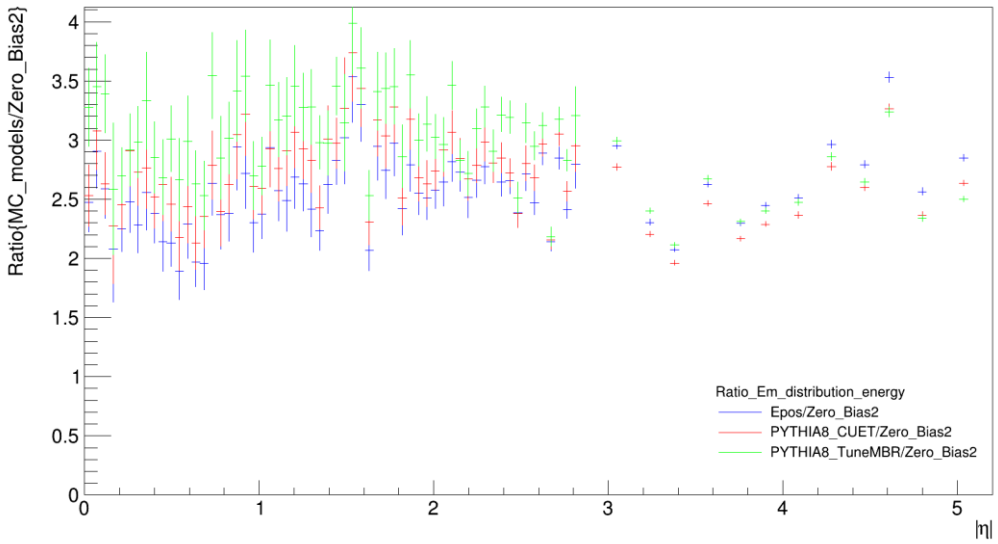

Fig. 6. Comparison between the ratio of all MC models (EPOS_LHC, PYTHIA8_CUET and PYTHIA8_MBR) to the real data (Zero_Bias2) in case of energy distribution of reconstructed electromagnetic particles

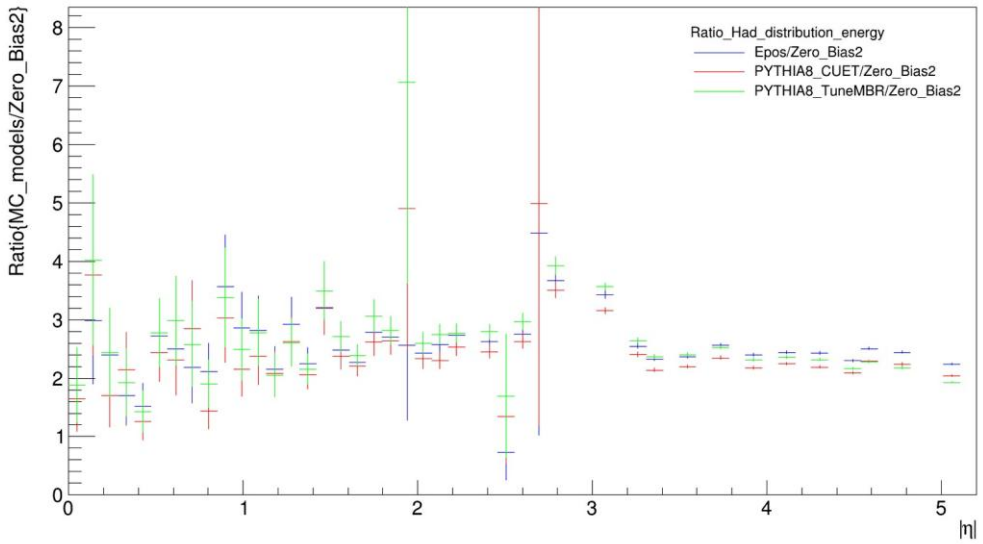

Fig. 7. Comparison between the ratio of all MC models (EPOS_LHC, PYTHIA8_CUET and PYTHIA8_MBR) to the real data (Zero_Bias2) in case of energy distribution of reconstructed hadronic particles

3. Results

The fact that this observable feature can be connected to several underlying particle generation mechanisms is also known to be of great importance for the interpretation of cosmic-ray air shower data.

It is better to go one step farther; it is beyond the LHC physics, Collisions happening in air showers scenario is the cosmic-ray particle happens in the atmosphere. where we have atmospheric hadron showers produced with cascade collisions in the atmosphere, it is the same physics particle produced in the hadronic channel and also in the neutrino and photon channel, but in the cosmic-air shower it is more produced particle than the LHC because the air shower produces charged pions so hadrons continue to fly in the atmosphere and they continue to collide and it is producing more collisions and so on. This is a multiplicative cascade that grows exponentially so it has a huge effect, but the same collisions in the channels produce photons also indirectly via resonance decay and pions. The photons do not produce further hadrons so their energy is removed, that is why it is important to know better. In Fig. 8 the (left-up-plot) shows the characteristic of electromagnetic energy distribution in generator level in eta range $0 \leq |\eta| \leq 6.6$, it is observed that the energy distribution of electromagnetic particles reaches the top in (CASTOR) region $5.2 \leq |\eta| \leq 6.6$, $\frac{1}{Nevts}\frac{dE}{d\eta}$=120 GeV in (PYTHIA8_MBR) case, $\frac{1}{Nevts}\frac{dE}{d\eta}$=144 GeV in (PYTHIA8_CUET) case and $\frac{1}{Nevts}\frac{dE}{d\eta}$=149 GeV in (EPOS-LHC) case. The (Right-up-plot) shows the characteristic of hadronic energy distribution in generator level and as observed also that the energy distribution of hadronic particles reaches the top in (CASTOR) region $5.2 \leq |\eta| \leq 6.6$, $\frac{1}{Nevts}\frac{dE}{d\eta}$=310 GeV in (PYTHIA8_MBR) case, $\frac{1}{Nevts}\frac{dE}{d\eta}$=320 GeV in (PYTHIA8_CUET) case and $\frac{1}{Nevts}\frac{dE}{d\eta}$=390 GeV in (EPOS-LHC) case. It is clear to show the different ratio R(gen_em/gen_had) in the generator particle level produced in different eta regions in figure 8 (bottom-plot), in the beginning, we see the particle produced in string fragmentation. And if we go more forward there are high-density effect become more observable and reach to the top in eta rang 5.2□|□|□6.6 (CASTOR region), so this plot explains the different produced particles in different eta regions. What we see in the (right-plot) in case of both (PYTHIA8_CUET) and (PYTHIA8_MBR) these curves are just flat in all eta ranges, it is clear because all of (PYTHIA8_CUET and PYTHIA8_MBR) makes one single particle production mechanism nothing else, every particle in (PYTHIA8_CUET and PYTHIA8_MBR) produced in the same way and has string fragmentation and nothing else. In the case of (EPOS-LHC), we see a transition in data so the particles ratio is not the same like PYTHIA8 case, which is different from $|\eta|=0$ to $|\eta|=6$; it is an interesting point because the changing in different model predictions shows what the data tells us if the data is flat or not flat. The two similar cases are not good enough to tell us the exactly correct models because of too much fluctuation. But it

..
is good to study the measurement data effects. The systematic effect of the yellow b and. Fluctuation is not been understood well until now, but there is no physics in that structure, maybe this is an effect of calorimeter noise, and maybe an effect of the (correction average) or maybe statistical in MC samples. It is obvious to study the characteristics of the electromagnetic and hadronic particles in the calorimeter level and their energy density dE/dη in eta range. It is shown in Fig. 9 and Fig. 10.

in Fig. 9 to study the energy distribution of reconstruction hadronic particles and the comparisons between 4 MC-modules (EPOS-LHC, PYTHIA8_CUET, PYTHIA8_MBR, and Zero-bias 1), as shown the energy increase smoothly with increasing in eta region with a sudden increase at |η|=3, this is where in CMS central brass-scintillator calorimeters stop, and the forward Quartiz-chrenkove calorimeters begin. We also observe some misses in hadrons particles in 2.0<|η|<2.8 region, in this region the hadron particles have lower energy than the other. This must be a combination of binning/calorimeter segmentation and dead material, but this is well reproduced by the detector MC, so we don't handle this specially. as shown in figure 10 the energy distribution of reconstruction electromagnetic particles, and the comparisons between 4 MC-modules (EPOS-LHC, PYTHIA8_CUET, PYTHIA8_MBR, and Zero-bias1), we observe that the characteristic of distribution energy of electromagnetic particle is a little as same as the characteristic of hadronic particles since the energy increase smoothly with increasing the eta value and the MC modules walk parallel with Zero_bias2, there is also a sudden increasing in energy in eta range around |η|=3.

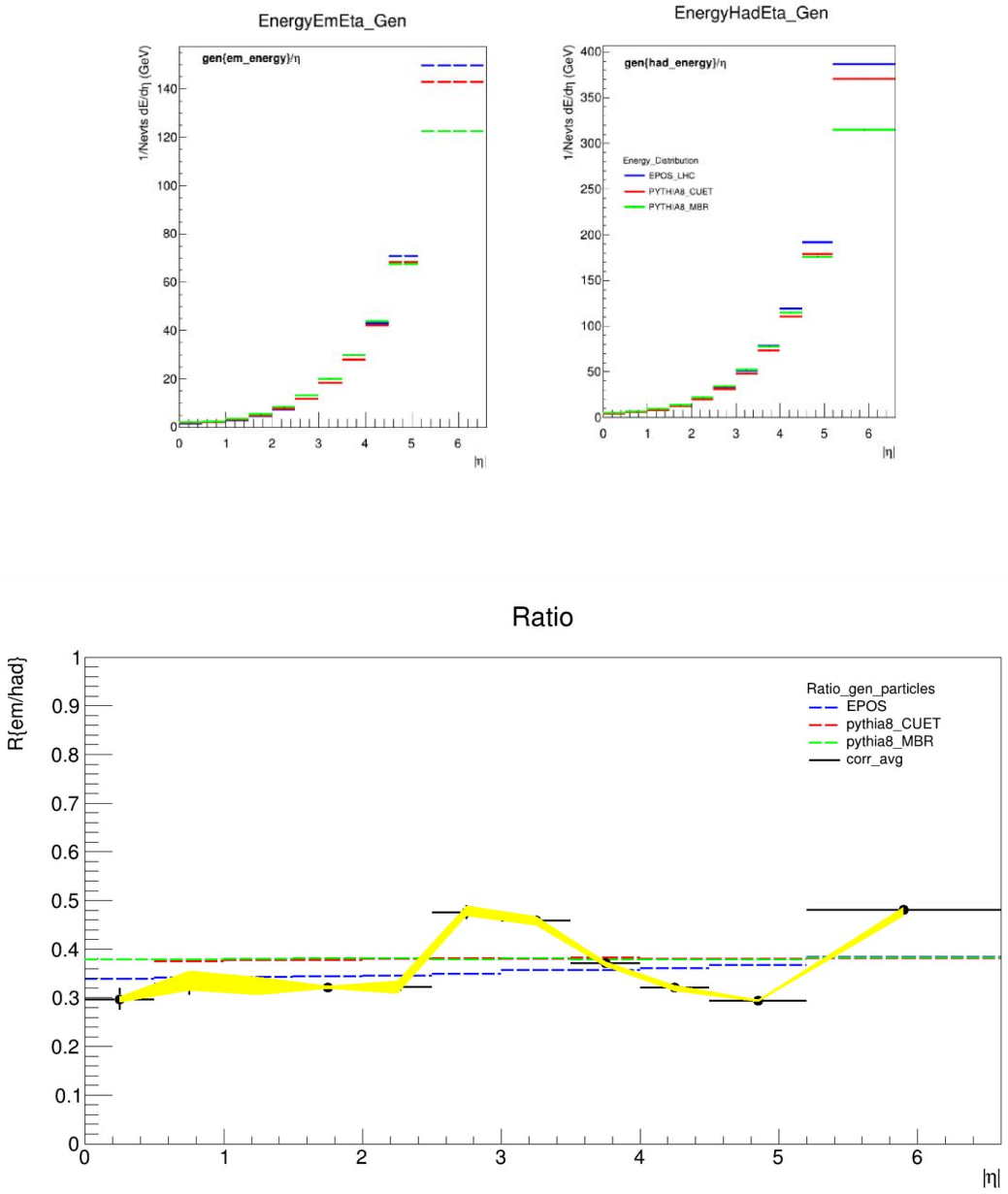

Fig. 8. (left-up-plot) comparison of electromagnetic energy distribution in generator level in eta range, (right-up-plot) hadronic energy distribution in generator level in eta range and (bottom-plot) the comparison of the ratio between electromagnetic and hadronic particles in generator level and the average of these corrections in eta range, the yellow band indicates the size of the model-dependent systematic uncertainly, the black bars are the statistical uncertainties.

..

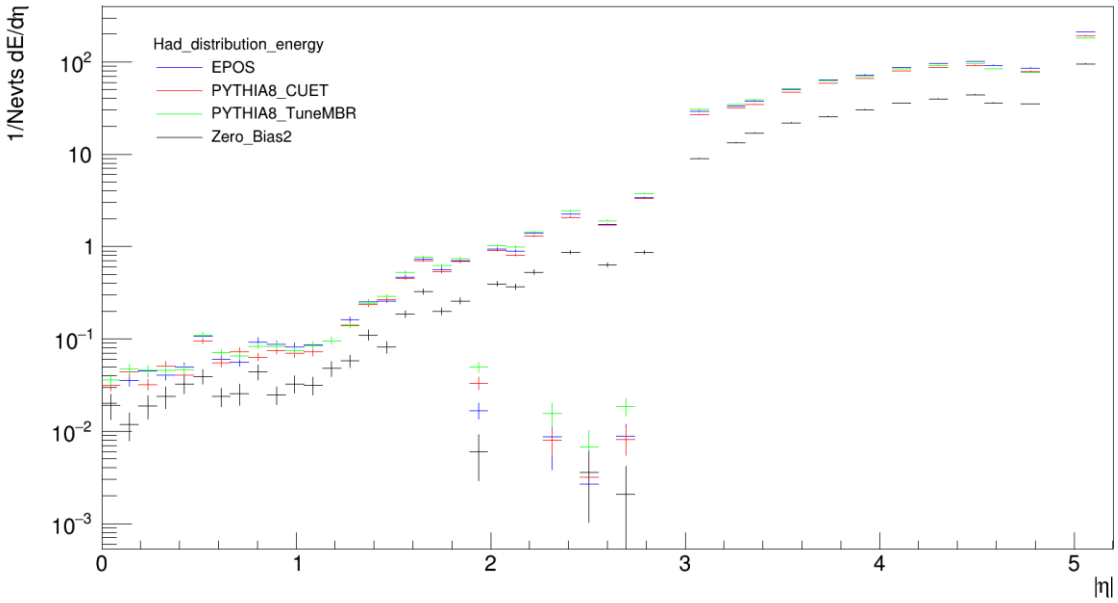

Fig. 9. Comparisons between 4 MC-models (EPOS-LHC, PYTHIA8_CUET, PYTHIA8_MBR, and Zero-bias 1), to study the reconstruction energy of hadronic particles in the calorimeter level.

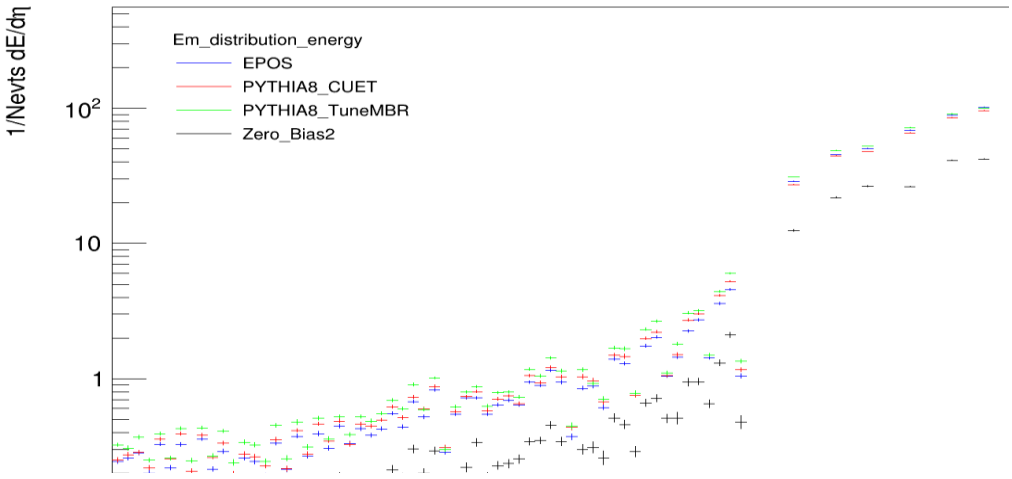

Fig. 10. Comparison between 4 MC-models (EPOS-LHC,PYTHIA8_CUET, PYTHIA8_MBR, and Zero-bias 1), to study the reconstruction energy of electromagnetic particles in the calorimeter level.

Conclusions

In this paper we study the spectra energy distribution for both of electromagnetic and hadronic particles real data collected with CMS detector including CASTOR at energy = 13 TeV and comparing with two different event generators (EPOS-LHC and PYTHIA8_CUET) in 11-eta-bins from eta-bin=0 to eta-bin=10,

The detector noise levels were measured for all calorimeters in eta-bins separately for electromagnetic and hadronic energies. Average energies are then measured above 5 times the noise level.

Several comparisons with MC simulations show that the facts are well-described. For both electromagnetic and hadronic particles, the MC was utilized to calculate the correction factors from detector-level to particle-level. In the future, the analysis might be improved even further by concentrating on those extra uncertainties. It was shown that the calorimeters of CMS taken all together and covering a very wide eta range from |0.0| to |6.6| may well be suited to provide further insights into hadronization and collective effects even in Zero Bias p-p collisions. While the analysis uncertainties are partly still a bit too large to make definitive observations and conclusions, there are hints that additional collective effects as included in EPOS are already visible in these data. However, currently those large uncertainties would not rule out the PYTHIA predictions which have no such collective effects included. The comparisons between the selected models were discussed in order to determine which model is more consistent with the real data, and which model is best suited to explain the particle data characteristics over a wide eta range.

References

[1] T. Sjöstrand and M. van Zijl, "Multiple parton-parton interactions in an impact parameter picture", Phys. Lett. B 188 (1987) 149, doi:10.1016/0370-2693(87)90722-2.

[2]T.Sjöstrand and M. van Zijl, "A multiple-interaction model for the event structure in hadron collisions", *Phys. Rev.* D 36 (1987) 2019, doi:10.1103/PhysRevD.36.2019.

[3]I.Borozan and M. H. Seymour, "An eikonal model for multiparticle production in hadron-hadron interactions", *JHEP* 09 (2002) 015,

doi:10.1088/1126-6708/2002/09/015, arXiv:hep-ph/0207283.

[4] T. Sjöstrand and P. Z. Skands, "Multiple interactions and the structure of beam remnants", *JHEP* 03 (2004) 053, doi:10.1088/1126-6708/2004/03/053, arXiv:hep-ph/0402078.

[5]CMS Collaboration, "First measurement of the underlying event activity at the LHC with □s = 0.9 TeV", *Eur. Phys. J. C* 70 (2010) 555,

doi:10.1140/epjc/s10052-010-1453-9, arXiv:1006.2083.

[6] CMS Collaboration,"Measurement of energy flow at large pseudorapidities in pp collisions at □s = 0.9 and 7 TeV", JHEP 11 (2011) 148 doi:10.1007/JHEP11(2011)148, arXiv:1110.0211. [Erratum: doi:10.1007/JHEP02(2012)055].

[7] ATLAS Collaboration, "Measurements of the pseudorapidity dependence of the total transverse energy in proton-proton collisions at □s = 7 TeV with ATLAS", JHEP 11 (2012) 033, doi:10.1007/JHEP11(2012)033, arXiv:1208.6256.

[8] LHCb Collaboration, "Measurement of the forward energy flow in pp collisions at □s = 7 TeV", *Eur. Phys. J. C* 73 (2013) 2421, doi:10.1140/epjc/s10052-013-2421-y, arXiv:1212.4755.

[9] J. Benecke, T. T. Chou, C.-N. Yang, and E. Yen, "Hypothesis of limiting fragmentation in high-energy collisions", Phys. *Rev.* 188 (1969) 2159, doi:10.1103/PhysRev.188.2159.

[10] J. Ruan and W. Zhu, "Particle multiplicities at energies available at the CERN Large Hadron Collider (LHC) and deviations from limiting fragmentation", *Phys. Rev. C* 81 (2010) 055210, doi:10.1103/PhysRevC.81.055210, arXiv:1005.2790.

..

[11] CMS Collaboration, “The CMS experiment at the CERN LHC”, *JINST* 3 (2008) S08004, doi:10.1088/1748-0221/3/08/S08004.

[12] T. Sjöstrand et al., “An Introduction to PYTHIA 8.2”, *Comput. Phys. Commun.* 191 (2015) 159, doi:10.1016/j.cpc.2015.01.024, arXiv:1410.3012.

[13] V. N. Gribov and L. N. Lipatov, “Deep inelastic ep scattering in perturbation theory”, *Sov. J. Nucl. Phys.* **15** (1972) 438. [Yad. Fiz. 15 (1972) 781].

[14] V. N. Gribov and L. N. Lipatov, “e + e pair annihilation and deep inelastic ep scattering in perturbation theory”, *Sov. J. Nucl. Phys.* **15** (1972) 675. [Yad. Fiz. 15 (1972) 1218].

[15] L. N. Lipatov, “The parton model and perturbation theory”, *Sov. J. Nucl. Phys.* **20** (1975) 94, doi:10.1016/0550-3213(79)90105-6. [Yad. Fiz. 20 (1974) 181].

[16] G. Altarelli and G. Parisi, “Asymptotic freedom in parton language*”, Nucl. Phys. B* **126** (1977) 298, doi:10.1016/0550-3213(77)90384-4.

[17] Y. L. Dokshitzer, “Calculation of the structure functions for deep inelastic scattering and e + e annihilation by perturbation theory in quantum chromodynamics.”, *Sov. Phys. JETP* **46** (1977) 641. [Zh. Eksp. Teor. Fiz. 73 (1977) 1216].

[18] B. Andersson, G. Gustafson, G. Ingelman, and T. Sjöstrand, “Parton fragmentation and string dynamics”, *Phys. Rept.* **97** (1983) 31, doi:10.1016/0370-1573(83)90080-7.

[19] CMS Collaboration, “Event generator tunes obtained from underlying event and multiparton scattering measurements”, *Eur. Phys. J. C* **76** (2016) 155, doi:10.1140/epjc/s10052-016-3988-x, arXiv:1512.00815.

[20] T. Pierog et al., “EPOS LHC: Test of collective hadronization with data measured at the CERN Large Hadron Collider”, *Phys. Rev. C* **92** (2015) 034906, doi:10.1103/PhysRevC.92.034906, arXiv:1306.0121.

[21] H. J. Drescher et al., “Parton-Based Gribov-Regge Theory”, *Phys. Rept.* **350** (2001) 93, doi:10.1016/S0370-1573(00)00122-8, arXiv:hep-ph/0007198.

[22] CMS Collaboration. "Measurement of energy flow at large pseudorapidities in pp collisions at s = 0.9 and 7 TeV", *JHEP* **11** (2011) 148, doi: 10.1007 / *JHEP* 11 (2011) 148, 10.1007 / JHEPO2 (2012) 055, arXiv: 1110. ozil. Erratum: JHEP02,055 (2012)